Article:

Wang, Sainan, Newland, Mike J., Rickard, Andrew R. orcid.org/0000-0003-2203-3471 et al. (11 more authors) (2025) Largely underestimated production of isoprene epoxydiols (IEPOX) through high-NO oxidation pathways in urban areas. npj Climate and Atmospheric Science. 256. ISSN 2397-3722

https://doi.org/10.1038/s41612-025-01151-4 npj | climate and atmospheric science

Article

Published in partnership with CECCR at King Abdulaziz University

https://doi.org/10.1038/s41612-025-01151-4

Largely underestimated production of isoprene epoxydiols (IEPOX) through high-NO oxidation pathways in urban areas

Sainan Wang[1,2], Mike J. Newland[3,4], Andrew R. Rickard[3,4], Jacqueline F. Hamilton[3,4], Thomas J. Bannan[5], Archit Mehra[5,8], Carl J. Percival[5,9], Freya A. Squires[4,10], Weiwei Hu[2], Wei Song[2], Yang Chen[6], Xiaoling Zhang[1], Liming Wang[7] & Xinming Wang[2] ✉

Isoprene is the dominant nonmethane volatile organic compound (VOC) emitted into the atmosphere globally, with important atmospheric chemistry impacts on air quality and climate. One crucial intermediate in its gas-phase oxidation is isoprene epoxydiol (IEPOX), which contributes significantly to the formation of secondary organic aerosols (SOA). It is generally accepted that IEPOX is efficiently formed in remote forested regions with a sufficiently low NO/HO_2 ratio. Here, we show that the oxidation of isoprene hydroxynitrates (IHN) can be an alternative, efficient, NO-driven pathway leading to the formation of IEPOX in urban areas where moderate to high NO concentrations exist. Field measurements from the megacity of Beijing show that this pathway contributes to more than 50% of IEPOX production during the morning and early afternoon. The results improve our understanding of the NO_x dependence of SOA formation in polluted areas, where anthropogenic emissions can significantly enhance biogenic SOA formation.

Isoprene (C_5H_8, 2-methyl-1,3-butadiene), the most abundant atmospheric nonmethane volatile organic compound (VOC) with global emissions of *ca.* 594 Tg year^{-1}, and a short lifetime of ~1–2 h, significantly impacts atmospheric chemistry on a global scale[1–3]. The gas phase degradation chemistry of isoprene greatly contributes to tropospheric ozone production and impacts the oxidizing capacity of the atmosphere by affecting photochemical cycles of NO_x and HO_x[4–6]. In addition, isoprene-derived secondary organic aerosols (SOA) can influence climate and human health[5,7]. The emission of isoprene is primarily from deciduous plants and typically varies with light flux and temperature, leading to large emissions in areas such as the Amazon rainforest and the southeastern US. Nevertheless, in urban areas with high coverage of urban forests and green spaces, large biogenic isoprene emissions can occur in the daytime, along with non-negligible anthropogenic sources such as vehicle exhausts[8–10].

The dominant daytime removal process of isoprene in the atmosphere is the reaction with the hydroxyl radical (OH; k_{OH} (298 K) = 1.0×10^{-10} cm^3 molecule^{-1} s^{-1})[11]. The initial addition of OH is followed by O_2 addition to form a hydroxyperoxy radical intermediate ($ISOPO_2$), of which there are six dominant isomers because of site-specific OH/O_2 additions[12,13]. Significant progress has been made in recent years in understanding the relative distribution of different $ISOPO_2$ isomers, which depends on their reaction rates with HO_2 and NO, and unimolecular isomerization (i.e. H-shift chemistry in Z-δ-$ISOPO_2$)[14–16]. The majority of $ISOPO_2$ will eventually undergo bimolecular reaction with either NO or HO_2. In environments with a sufficiently low NO/HO_2 ratio, $ISOPO_2$ predominantly reacts with HO_2 radicals to form isoprene hydroxyhydroperoxides (ISOPOOH), which can be further oxidized by OH radicals to produce isoprene epoxydiols (IEPOX), accompanied by OH recycling (Fig. 1)[5]. Laboratory studies and field measurements have demonstrated that IEPOX can serve as an

---

[1]Plateau Atmosphere and Environment Key Laboratory of Sichuan Province, School of Atmospheric Sciences, Chengdu University of Information Technology, Chengdu, China. [2]State Key Laboratory of Organic Geochemistry and Guangdong Key Laboratory of Environmental Protection and Resources Utilization, Guangzhou Institute of Geochemistry, Chinese Academy of Sciences, Guangzhou, China. [3]Wolfson Atmospheric Chemistry Laboratories, Department of Chemistry, University of York, Heslington, UK. [4]National Centre for Atmospheric Science, Department of Chemistry, University of York, Heslington, UK. [5]School of Earth, Atmospheric and Environmental Sciences, University of Manchester, Manchester, UK. [6]Center for the Atmospheric Environment Research, Chongqing Institute of Green and Intelligent Technology, Chinese Academy of Sciences, Chongqing, China. [7]School of Chemistry & Chemical Engineering, South China University of Technology, Guangzhou, China. [8]Present address: Methods Analytics, London, UK. [9]Present address: Jet Propulsion Laboratory, California Institute of Technology, Pasadena, CA, USA. [10]Present address: British Antarctic Survey, Natural Environment Research Council, Cambridge, UK.
✉e-mail: wangxm@gig.ac.cn

Fig. 1 | Main reactions of gas-phase oxidation of isoprene in remote forest and urban regions using β-1,2-ISOPO$_2$ as an example. (β-1,2-ISOPO$_2$ is formed via OH-addition to the C$_1$- position and O$_2$-addition to the C$_2$- position).

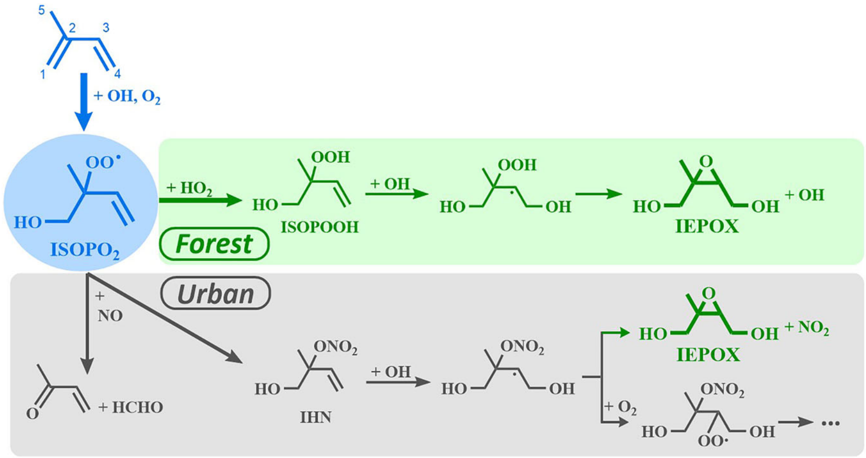

important SOA precursor via aerosol phase reactions[17–19], and IEPOX-derived SOA accounts for 6–36% of organic aerosols in forested areas[20]. As NO increases, the HO$_2$-pathway to form IEPOX via ISOPOOH is suppressed, and instead, ISOPO$_2$ species react with NO, forming methyl vinyl ketone (MVK) and methacrolein (MACR) as the two main stable carbonyl products, with the latter being considered as a possible SOA precursor owing to reactive uptake of subsequent oxidation products into particles[18,21–23]. The overall NO$_x$ dependence of isoprene SOA yields in polluted regions has not yet been fully elucidated and remains somewhat controversial. Previous laboratory studies have reported the non-linear response of isoprene-derived SOA to elevated NO$_x$, but cannot explain the significant SOA yield at high NO$_x$[22,24–26]. Several field measurements have indicated that the formation of SOA can be enhanced by NO$_x$ in isoprene-rich areas[27–29]. Large amounts of IEPOX-derived SOA tracers have been observed in urban areas where high levels of NO can suppress IEPOX formation via the HO$_2$- pathway[30–36]. In highly industrialized areas in China, such as the Pearl River Delta (PRD) region and eastern cities in China, the concentration of 2-methyltetrols (typical IEPOX-derived SOA tracers) in SOA during the summer were observed on average to be 91.5 ng cm^{-3} and 89.0 ng cm^{-3}, respectively[35,36]. This indicates that there may be alternative pathways leading to IEPOX production in more polluted urban regions.

The reaction of ISOPO$_2$ with NO can also form isoprene hydroxynitrates (IHN in Fig. 1), with the total yield varying from 0.04 to 0.15[15,37–39]. The formation of IHN, as a radical chain-terminating step sequesters NO$_x$, reducing local O$_3$ production. In recent years, IHN and IHN-derived dinitrates have been observed in the ambient atmosphere[40,41], and a recent chamber study has suggested that such lower volatility nitrates derived from isoprene might make a greater contribution to SOA formation than previously thought[42]. However, due to the difficulty in the synthesis of IHN standards and the quantification of multi-functionalized products, the current understanding of IHN chemistry remains uncertain.

In the daytime, the major removal process for IHN is oxidation by OH radicals, with rate constants in the range of (3–11) × 10^{-11} cm^3 molecule^{-1} s^{-1} for the different IHN isomers[12]. Note that 1,2-IHN might be an exception as it can undergo condensed-phase hydrolysis rapidly, depending on atmospheric liquid water volume[43]. In general, OH addition to the double bond forms an IHN-OH adduct, which subsequently combines with O$_2$ to form a peroxy radical (Fig. 1). Alternatively, Jacobs et al. suggested that the IHN-OH adduct might form IEPOX by intramolecular isomerization[44]. The researchers conducted flow tube experiments using synthesized 4,3-IHN in the pressure range of 50–400 Torr and reported an IEPOX yield of 71% at 50 Torr, corresponding to a yield of 13% when extrapolated to atmospheric pressure (760 Torr). However, IHN chemistry has not received much attention over the past few decades, and the IEPOX formation mechanism from IHN has been ignored in field measurements and modeling studies. In their 2018 review on gas-phase isoprene chemistry, Wennberg et al. suggest a total yield of 0.14 for IEPOX formation from OH reactions with all IHN isomers[12].

In this paper, we reassess the reactions of the dominant IHN isomers with OH radicals using high-level theoretical calculations, and carry out model simulations for comparison with ambient observations. The calculations confirm that the energized IHN-OH* adduct can undergo intramolecular isomerization to form considerable amounts of IEPOX and NO$_2$, indicating that the currently acknowledged yield of IEPOX from the IHN reaction with OH might be underestimated. The updated chemistry is incorporated into a box model using the full isoprene oxidation scheme from the MCMv3.3.1[13]. The model is then constrained to measurements from Beijing in the summer of 2017 to demonstrate the relative contributions of the IHN and ISOPOOH pathways to IEPOX formation. It is well accepted that IEPOX can be formed significantly from the oxidation of ISOPOOH (formed via ISOPO$_2$ + HO$_2$) in low NO$_x$ regions such as remote forests. Here we show that the oxidation of IHN (formed via ISOPO$_2$ + NO) can also be an important formation pathway of IEPOX in high-NO urban environments, which needs to be considered seriously in future ambient measurements and atmospheric science and air quality policy modeling. Considering the ubiquity of isoprene in the atmosphere and its large global emissions, our findings could help to improve assessments of isoprene-derived SOA formation mechanisms and its contribution to photochemical ozone formation, especially in urban areas.

Results

In the presence of NO$_x$, the OH-initiated oxidation of isoprene can produce six hydroxy nitrate isomers, including the two major isomers β-1,2-IHN and β-4,3-IHN, and four minor isomers (E/Z)-δ-1,4-IHN and (E/Z)-δ-4,1-IHN[12]. Given the chemical similarity of E- and Z- δ-IHNs shown in a previous study, the two types of isomers are expected to react identically[12]. In the present work, we carried out theoretical calculations and kinetics modeling using the four IHN isomers shown in Fig. 2a.

Yields of IEPOX from OH reactions with IHNs

The reaction of IHNs with OH radicals proceed mainly as site-specific OH additions to the double bond. Taking β-1,2-IHN as an example (Fig. 2b), when OH is added at the C$_4$- position, the adduct can either (i) combine with O$_2$ to form a peroxy radical or (ii) intramolecularly isomerize to an IEPOX and release NO$_2$; the two reactions compete with each other. However, such isomerization pathways cannot occur when OH is added at the C$_3$- position. It should also be noted that OH radicals can alternatively abstract an H atom from the methyl group, which is a minor pathway. Taking both aspects into consideration, we calculate all types of the initiating reaction steps of IHN isomers. Table 1 shows the branching ratios of the OH-addition pathway

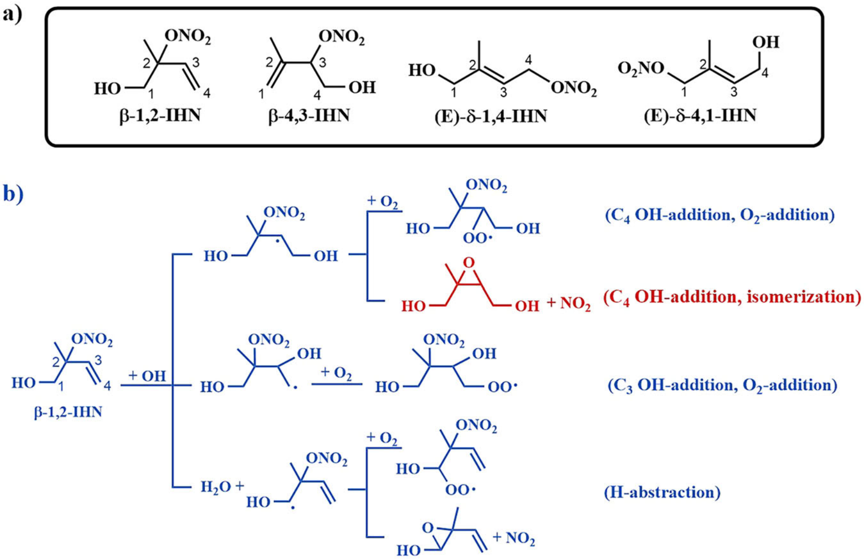

Fig. 2 | Possible reaction mechanisms of IHN. **a** Four IHN isomers investigated in this study. **b** Possible pathways of OH reactions with specific IHN isomers using β-1,2-IHN as an example (IEPOX formation pathway is highlighted in red).

Table 1 | Yields of IEPOX from IHN + OH reaction in this work and previous work by Wennberg et al.

	[a](OH-initiated)	[b](Isomerization)	[c](IEPOX)	
			This work	Wennberg et al.[12]
β-1,2-IHN	0.61	0.62	0.38	0.15
β-4,3-IHN	0.99	0.34	0.34	0.13
δ-1,4-IHN	0.77	0.65	0.50	0.04
δ-4,1-IHN	0.36	0.90	0.32	0.08

[a] $_{\text{(OH-initiated)}}$ the branching ratios of the OH-addition pathway that can potentially form IEPOX.

[b] $_{\text{(Isomerization)}}$ branching ratios of the IEPOX formation pathway from available IHN-OH adducts.

[c] $_{\text{(IEPOX)}}$ yields of IEPOX from IHN oxidation by OH, considering OH abstractions and other OH additions that cannot form IEPOX. Y $_{\text{(IEPOX)}}$ is the product of Φ $_{\text{(OH-initiated)}}$ and Γ $_{\text{(Isomerization)}}$ in this work.

(Φ $_{\text{OH-initiated}}$) that can potentially form IEPOX from β-1,2-IHN, β-4,3-IHN, δ-1,4-IHN and δ-4,1-IHN, which are 0.61, 0.99, 0.77 and 0.36, respectively. Detailed reaction energies are available in Supplementary Table S2.

Figure 3 depicts the potential energy surface of OH reactions with four IHN isomers for the isomerization process. Comprehensive potential energy surface diagrams for all isomers are presented in Supplementary Fig. S1. The reaction energies shown here are obtained at the RHF-RCCSD(T)-F12a level with the basis set cc-pVDZ-F12 (see Methods). T1 diagnostics were used to check the multireference characteristics of the wave functions. In our calculations, all critical reaction steps exhibited T1 diagnostic values below 0.022, thereby confirming the reliability and robustness of the applied computational methodologies (Supplementary Table S1). As shown in Fig. 3, four transition states (TS-OH) for OH additions are submerged under the corresponding reactants, and four IHN-OH adducts (P-OH) are formed with energy released of >100 kJ/mol. P-OHs can combine with O_2 to form normal peroxy radicals (P-OH-OO), which are expected to form alkoxy radicals in the presence of NO and predominantly followed by fragmentation. Alternatively, the P-OHs can intramolecularly isomerize to IEPOX and NO_2 over the barrier of 50~70 kJ/mol based on our calculations. We paid close attention to quantifying the isomerization process influenced by multiple conformers. Multiple conformers are searched by systematically changing the dihedral angles. Structures of conformers were initially optimized at B3LYP or M06-2X levels with basis set 6-31 + G(d,p) or 6-31 G(d), and geometries of low-energy conformers (within 10 kJ/mol above the lowest-energy conformers) are further refined at M06-2X/6-311 + + G(2df,2p) levels. Then the low-energy conformers and transition states within 5 kJ/mol above the lowest-energy conformers are submitted for CCSD(T)-F12a/cc-pVDZ-F12 calculations and included in RRKM-ME calculations to obtain the yields of P-OH-OO and IEPOX from the two different pathways available for P-OH (more details can be found in Methods). The predicted branching ratios forming IEPOX from isomerization of the four P-OH isomers studied here (β-1,2-IHN, β-4,3-IHN, δ-1,4-IHN and δ-4,1-IHN) at 298 K and 760 Torr are 0.62, 0,34, 0.65 and 0.90, respectively (Table 1). Such unimolecular isomerization reactions from the energized OH-adduct* to IEPOX are pressure-dependent, and as such the relative yield of IEPOX would decrease at higher pressures, as shown in Supplementary Fig. S4. Considering calculated fractions of available OH additions that potentially form IEPOX, the final yields of IEPOX from OH reactions with the four IHN isomers are 0.38, 0.34, 0.50 and 0.32, respectively (Table 1), which are considerably higher than that recommended by Wennberg et al.[12].

The results presented here could help to explain the observed imbalanced molar yield of products from subsequent reactions of P-OH-OO (O_2 addition channel) in the presence of NO. Jacobs et al. reported an IEPOX yield of 0.13 for β-4,3-IHN, and yields of 0.70 and 0.17 for two other products, methyl vinyl ketone hydroxy nitrate (MVKN) and hydroxyacetone (HAC), from different fragmentations of the P-OH-O radical, respectively[44]. However, Kurtén et al. carried out theoretical calculations showing that the cleavage-forming HAC is unavailable[45], which is consistent with our results in this study (Supplementary Table S3). Here we propose that the HAC observed by Jacobs et al. might be formed from second-generation reactions of IEPOX with OH radicals, which has been confirmed as one of the major products from gas-phase IEPOX oxidation in previous studies[46,47]. As a consequence, the Jacobs et al. yield of IEPOX from IHN oxidation would be underestimated. Similarly, Lee et al. obtained a yield of 0.10 for HAC in a chamber study of the oxidation of isoprene-derived

Fig. 3 | Potential energy surface of OH reactions with four IHN isomers regarding the isomerization process. Transition states (TS-OH) for OH additions are submerged under the corresponding reactants, and negative barriers may arise from the formation of pre-reactive complexes (PRC). Each IHN isomer reacts with OH to form the corresponding IHN-OH adduct (P-OH), which combines with O_2 to form a peroxy radical (P-OH-OO) or intramolecularly isomerizes to form IEPOX and NO_2.

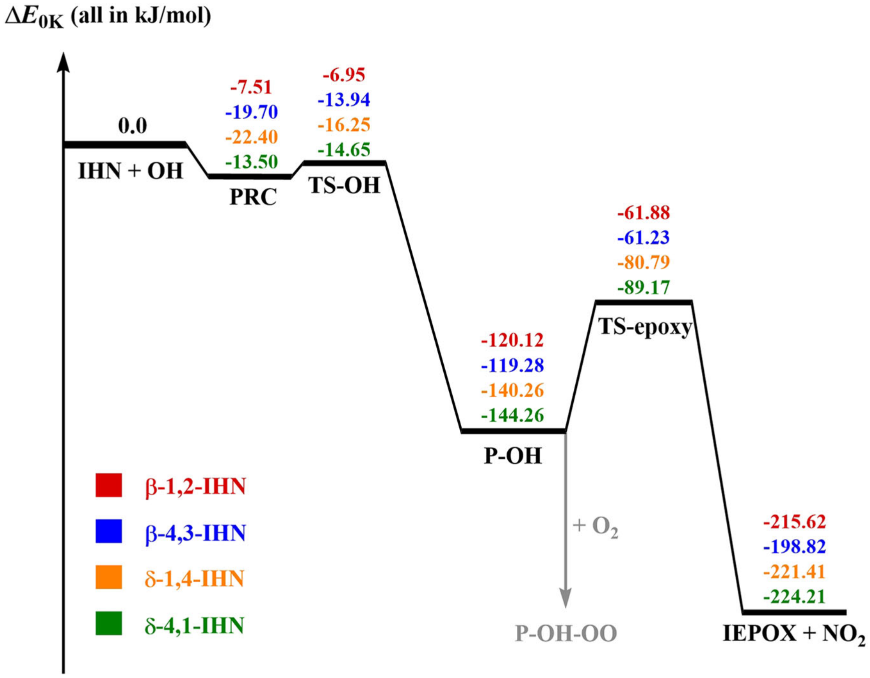

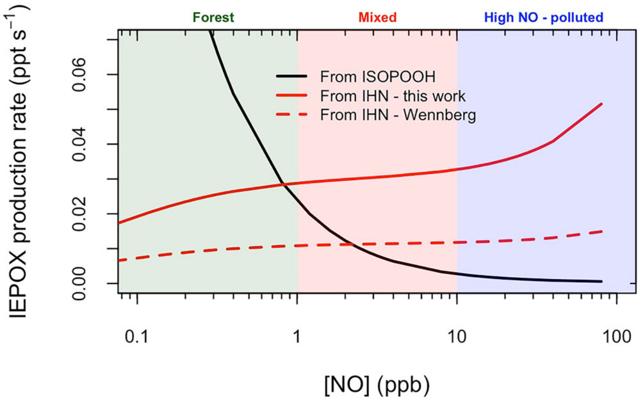

Fig. 4 | The steady state IEPOX production rate from the oxidation of ISOPOOH and IHN, respectively, as a function of NO concentration. Assuming $[C_5H_8]$ = 1 ppb and $[HO_2] = 5 \times 10^8 cm^{-3}$. IEPOX yields in IHN are taken from the calculation results in this work and previous work from Wennberg et al.[12]. Shaded regions show typical NO mixing ratio ranges for forested, mixed and urban polluted environments.

hydroxy nitrates, which might be explained by the same process[48]. Moreover, Lee et al. also investigated fragmentation products from the OH-oxidation of δ-1,4-IHN and observed a higher yield of HAC than of its co-product (ethanal nitrate), which might also be due to the OH reaction with the primary IEPOX formed.

Uncertainty analysis of computational results

Our computational results entail inherent uncertainties arising from multiple variables. We systematically assessed three primary uncertainty sources: (1) energy calculations employing the CCSD(T)-F12a/cc-pVDZ-F12 method; (2) energy transfer parameter in RRKM-ME calculation ($\langle \Delta E \rangle_{down}$); (3) O_2 addtion rate coefficients. First, the uncertainty of predicted energies using CCSD(T)-F12a/cc-pVDZ-F12 method is ~1 kcal/mol. For energy uncertainties, RRKM-ME simulations were conducted under two boundary conditions: (i) lowering the energy of P-IHN-OH by 2 kJ/mol and elevating the energy of transition states by 2 kJ/mol (ii) elevating the energy of P-IHN-OH by 2 kJ/mol and lowering the energy of transition states by 2 kJ/mol (Supplementary Section S4 in SI). Resulting IEPOX yields from 1,2-/4,3-/1,4-/4,1- IHN-OH adducts spanned 0.41–0.81, 0.19–0.55, 0.44–0.84, and 0.74–0.9, respectively (Supplementary Table S5). Second, a higher $\langle \Delta E \rangle_{down}$ input in the energy transfer model would adversely affect the formation of IEPOX. With $\langle \Delta E \rangle_{down}$ of 250 cm^{-1} (a relatively elevated value), the yield of IEPOX presented in Table 1 represent lower threshold values. If lower $\langle \Delta E \rangle_{down}$ values were employed, a higher yield of IEPOX could be anticipated (see Supplementary Section S3 in SI). Third, the O_2 addition rate coefficient to P-IHN-OH was fix at 6.0 $\times 10^{-12}$ cm^3 $molecule^{-1}$ s^{-1} (literature-consistent). Sensitivity tests across 1.0 $\times 10^{-12}$ to 1.0 $\times 10^{-11}$ cm^3 $molecule^{-1}$ s^{-1} indicated negligible impacts on IEPOX yield.

Box modeling of IEPOX formation from NO_x- and HO_2- pathways

Based on the calculations presented, the reactions of IHN (formed from $ISOPO_2 + NO$) will contribute significantly to the formation of IEPOX in the atmosphere, in addition to the more recognized low-NO pathway via ISOPOOH (formed from $ISOPO_2 + HO_2$). In the ambient atmosphere, the NO/HO_2 ratio can vary greatly under different environmental conditions and times of day, such that both the NO and HO_2 pathways may be important. Thus, we carried out model simulations to understand the role of NO in IEPOX formation. Figure 4 shows the production rate of IEPOX from ISOPOOH + OH and IHN + OH as a function of NO concentration. The production rate is calculated for the system at steady state assuming 1 ppb of C_5H_8, $[OH] = 9 \times 10^6 cm^{-3}$ (daytime peak in mean diurnal [OH] measured during campaign), and $[HO_2] = 5 \times 10^8 cm^{-3}$. Plots for $[HO_2] = 1 \times 10^8$ and $1 \times 10^9 cm^{-3}$ are shown in the SI, and while the cross-over points of IEPOX production from ISOPOOH vs. IHN change, the ratio between the IEPOX yields from IHN calculated using the values from Wennberg et al. and from this work remains the same.

The black line in Fig. 4 represents the production of IEPOX from ISOPOOH, which decreases dramatically with increasing NO concentrations. In heavily polluted regions, the contribution of this pathway is negligible compared to production via IHN. The red solid line and the red dashed line show the IEPOX production rate from IHN using IEPOX yields from this work and the previous study[12], respectively. The production rate from this work is approximately a factor of ~2.5 higher than that from Wennberg et al. It is worth noting that the cross-over point, at which the

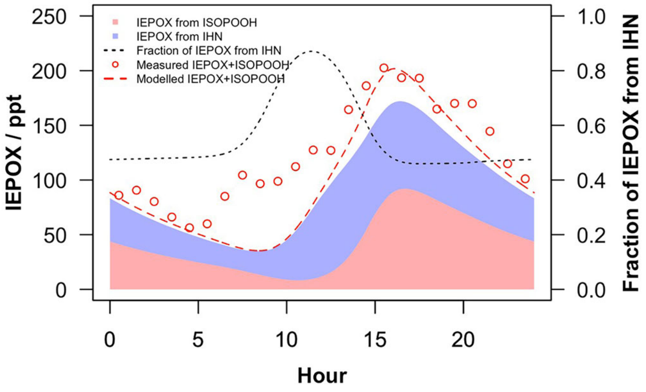

Fig. 5 | Production of IEPOX from ISOPOOH + OH and IHN + OH, constrained to the campaign average diurnal profiles of IHN, C_5H_8, OH, HO_2, NO, measured in Beijing (see SI). Black dash line: fraction of IEPOX derived from IHN + OH.

IEPOX production from IHN equals that from ISOPOOH, occurs at [NO] ~1 ppb using the IEPOX yields from this work (which varies with [HO_2]). The transition region between background and lightly polluted conditions, approximately 0.8 ppb of NO in central Amazonia in the wet season, is very sensitive to isoprene photochemistry related to the production of IEPOX-derived SOA[49]. Moreover, the sensitivity in this region has also been shown to be important even in polluted megacities, such as Beijing, where NO concentrations can routinely be suppressed to <1 ppb through the afternoon[50].

A case study of IEPOX formation in urban areas

A box model was constrained to mean diurnal cycles of isoprene, OH, HO_2, NO and IHN measured in Beijing between 17 May and 24 June 2017 as part of the APHH-Beijing field campaign[50–52]. A time-of-flight chemical ionization mass spectrometer (ToF-CIMS) using an iodide ionization system was deployed to measure IEPOX ($C_5H_{10}O_3$), ISOPOOH ($C_5H_{10}O_3$) and IHN ($C_5H_{10}O_4N$), and the method of field calibration was described in a previous work[50]. Figure 5 shows the relative contributions of the ISOPOOH and IHN pathways to the overall modeled IEPOX concentrations using the IEPOX yields from IHN calculated in this work. Using the revised IEPOX yields, between 08:00 and 14:00 more than half of the IEPOX present is attributable to the IHN + OH reaction, up to a maximum of 85% at 11:00. The IEPOX present from ISOPOOH during this time period is residual, leftover from the previous day. In the late afternoon (15:00–18:00), the formation from ISOPOOH becomes increasingly important under the low NO conditions seen in Beijing. However, during this period, more than 40% of the IEPOX present is still attributable to the IHN + OH reaction.

Discussion

Owing to its high reactivity and solubility, IEPOX is well known to contribute to aerosol formation[12]. While the reaction of ISOPOOH with OH has been shown to be a very efficient route to IEPOX, it has been established that IEPOX can also be formed from the reaction of IHN + OH[44]. The high-level theoretical calculations performed in this study suggest that the IEPOX yields from this reaction are currently underestimated in models and highlight the potential importance of IEPOX production from the IHN + OH reaction to the total IEPOX burden. In the IHN + OH reaction, IEPOX formation proceeds through the epoxidation of β-nitrooxy alkyl radicals. Although similar radicals are also formed in NO_3-initiated reactions of alkenes (e.g., isoprene + NO_3), epoxidation pathways rarely occur in those cases. The primary reason for this difference is that the OH addition to IHN is significantly more exothermic, producing β-nitrooxy alkyl radicals with substantially greater internal energy and thus promoting their unimolecular epoxidation (see Supplementary Section S5). It should be noted that our computational results are subject to inherent uncertainties from collision parameters and energy calculations. With $\langle \Delta E \rangle_{down}$ of 250 cm^{-1} (a relatively elevated value), the yield of IEPOX predicted in this study (0.62, 0.34, 0.65 and 0.90 for 1,2-/4,3-/1,4-/4,1- IHN-OH adducts, respectively) represent lower threshold values (see Supplementary Section S3 in SI). With the uncertainty of predicted energies of ~1 kcal/mol, the IEPOX yields from 1,2-/4,3-/1,4-/4,1- IHN-OH adducts are predicted as $0.62^{+0.19}_{-0.21}, 0.34^{+0.21}_{-0.15}, 0.65^{+0.19}_{-0.21}, 0.90^{+0.08}_{-0.16}$, respectively (Supplementary Section S4 in SI).

Using measurements from the megacity of Beijing, it is shown that IHN + OH can dominate IEPOX production during the morning and early afternoon. Note that for the NO_3-dominated chemistry during nighttime, recent studies have reported that epoxidation reactions of nitrate alkoxy radicals play a role in the NO_3 oxidation of isoprene[53–55]. In these cases, epoxide formation occurs via ring-closure reaction of alkoxy radicals, potentially contributing to isoprene-derived SOA at night. The work presented here highlights that IHN oxidation can be an important formation pathway of IEPOX in urban areas with moderate to high NO concentrations, improving our understanding of the NO_x dependence of SOA formation in polluted areas and may explain the high concentrations of IEPOX-derived tracers observed in heavily polluted areas.

Methods

Theoretical methods

All the molecular structures were optimized at the level of DFT-M06-2X/6-311++G(2df,2p) using the Gaussian 09 suite of programs[56]. The optimized structures were submitted to electronic energies calculations using the explicitly correlated CCSD(T)-F12a (F12) method[57] with cc-pVDZ-F12 basis set, all using the restricted open-shell wave functions for the radical species. The F12 calculations were performed by using the Molpro 2015 package[58].

The reaction rate coefficients of the unimolecular reactions were calculated using the unimolecular rate theory coupled with the energy-grained master equation for collisional energy transfer (RRKM-ME)[59], which were carried out using the Mesmer code[60]. A single exponential-down model was used to approximate the collisional energy transfer with $\langle \Delta E \rangle_{down}$ of 250 cm^{-1}. The collisional parameters were estimated using the method of Gilbert and Smith[61], and the asymmetric Eckart model was used for the tunneling correction factors[62]. The rate coefficient of O_2 addition to the IHN-OH adduct (P-OH) was set to be a reference value of 6.0×10^{-12} cm^3 $molecule^{-1}$ s^{-1} according to previous studies[63].

Multi-conformers searching and description in Master Equation analysis

In this work, multi-conformers searching was executed in three stages:

Stage 1: Initial conformer search by systematically varying all the dihedral angles, optimize them initially at B3LYP or M06-2X levels with basis set 6-31 + G(d,p) or 6-31 G(d);

Stage 2: Refine geometries of the low-energy conformers within 10 kJ/mol above the lowest-energy conformers at M06-2X/6-311++G(2df,2p) level;

Stage 3: Calculate the electronic energy at CCSD(T)-F12a/cc-pVDZ-F12 level for conformers within 5 kJ/mol above the lowest-energy conformers.

Taking 1,2-IHN-4OH as an example, the numbers of conformers are 486, 101, and 5 at each stage; and for transition states from 1,2-IHN-4OH to IEPOX, the numbers of conformers are 81, 30, and 2. Then we included the low-energy conformers of P-IHN-OH and their corresponding transition states for IEPOX formation using a rigid-rotor harmonic-oscillator approximation in RRKM-ME calculations as, IHN + OH → (Low-energy conformers of IHN-OH intermediates, and assume equilibrium between them) → IEPOX or IHN-OH-OO. Final RRKM-ME calculation includes 5 conformers for 1,2-IHN-4OH (within 5 kJ/mol of energy to the lowest-energy conformer) and 2 transition states (within 5 kJ/mol of energy to the lowest transition states). Low energy barriers between 1,2-IHN-4OH conformers are included in RRKM-ME to ensure the rapid equilibria between conformers. Molecular coordinates of the intermediates and transition states used in RRKM-ME calculations have been included in Supplementary Section S6 in SI.

Box modeling and field measurements

We carried out box modeling with AtChem (version 1)[64] using the near-explicit chemical mechanism of MCMv3.3.1. The isoprene mechanism was updated as detailed in Supplementary Table S6 to calculate IEPOX production rates under different NO/HO_2 ratios, using IHN + OH yields from this work and Wennberg et al.[12].

A box model was constrained to mean diurnal cycles of isoprene, OH, HO_2, NO, and IHN measured in Beijing between 17 May and 24 June 2017 as part of the APHH-Beijing field campaign[50–52]. A time-of-flight chemical ionization mass spectrometer (ToF-CIMS) using an iodide ionization system was deployed to measure IEPOX ($C_5H_{10}O_3$), ISOPOOH ($C_5H_{10}O_3$) and IHN ($C_5H_{10}O_4N$), and the method of field calibration was described in a previous work[50]. The measured campaign mean diurnal cycles of isoprene, OH, HO_2, NO, and IHN are shown in Supplementary Fig. S8. The measured IHN was assumed to consist of 65% ISOPBNO3 (MCM name) and 35% ISOPDNO3, based on modeling and field observations[65]. A rate of 3×10^{-5} s^{-1} was used for the loss of IEPOX to aerosol uptake. This rate is known to be very sensitive to aerosol acidity[66] and can range from an IEPOX lifetime of ~ 2 h up to a day or more[67]. The rate used here gives a lifetime against aerosol uptake of 9 h and was derived from fitting to the diurnal mean measured IEPOX + ISOPOOH signal during the Beijing campaign. The relative contribution of the IHN + OH and ISOPOOH + OH pathways is not sensitive to this parameter.

Data availability

Data is provided within the manuscript or supplementary information files.

Received: 7 December 2024; Accepted: 23 June 2025;

References

1. Guenther, A. B. et al. The Model of Emissions of Gases and Aerosols from Nature version 2.1 (MEGAN2.1): an extended and updated framework for modeling biogenic emissions. *Geosci. Model. Dev.* **5**, 1471–1492 (2012).
2. Atkinson, R. & Arey, J. Gas-phase tropospheric chemistry of biogenic volatile organic compounds: a review. *Atmos. Environ.* **37**, S197–S219 (2003).
3. Sindelarova, K. et al. Global data set of biogenic VOC emissions calculated by the MEGAN model over the last 30 years. *Atmos. Chem. Phys.* **14**, 9317–9341 (2014).
4. Chameides, W. L., Lindsay, R. W., Richardson, J. & Kiang, C. S. The role of biogenic hydrocarbons in urban photochemical smog: Atlanta as a case study. *Science* **241**, 1473–1475 (1988).
5. Paulot, F. et al. Unexpected epoxide formation in the gas-phase photooxidation of isoprene. *Science* **325**, 730–733 (2009).
6. Paulot, F., Henze, D. K. & Wennberg, P. O. Impact of the isoprene photochemical cascade on tropical ozone. *Atmos. Chem. Phys.* **12**, 1307–1325 (2012).
7. Claeys, M. et al. Formation of secondary organic aerosols through photooxidation of isoprene. *Science* **303**, 1173–1176 (2004).
8. Borbon, A. et al. An investigation into the traffic-related fraction of isoprene at an urban location. *Atmos. Environ.* **35**, 3749–3760 (2001).
9. Wang, J.-L. et al. Biogenic isoprene in subtropical urban settings and implications for air quality. *Atmos. Environ.* **79**, 369–379 (2013).
10. Zhang, B., Xie, G., Gao, J. & Yang, Y. The cooling effect of urban green spaces as a contribution to energy-saving and emission-reduction: a case study in Beijing, China. *Build. Environ.* **76**, 37–43 (2014).
11. Atkinson, R. Gas-phase tropospheric chemistry of volatile organic compounds .1. Alkanes and alkenes. *J. Phys. Chem. Ref. Data.* **26**, 215–290 (1997).
12. Wennberg, P. O. et al. Gas-phase reactions of isoprene and its major oxidation products. *Chem. Rev.* **118**, 3337–3390 (2018).
13. Jenkin, M. E., Young, J. C. & Rickard, A. R. The MCM v3.3.1 degradation scheme for isoprene. *Atmos. Chem. Phys.* **15**, 11433–11459 (2015).
14. Peeters, J., Muller, J. F., Stavrakou, T. & Nguyen, V. S. Hydroxyl radical recycling in isoprene oxidation driven by hydrogen bonding and hydrogen tunneling: the upgraded LIM1 mechanism. *J. Phys. Chem. A.* **118**, 8625–8643 (2014).
15. Teng, A. P., Crounse, J. D. & Wennberg, P. O. Isoprene peroxy radical dynamics. *J. Am. Chem. Soc.* **139**, 5367–5377 (2017).
16. Wang, S., Riva, M., Yan, C., Ehn, M. & Wang, L. Primary formation of highly oxidized multifunctional products in the OH-initiated oxidation of isoprene: a combined theoretical and experimental study. *Environ. Sci. Technol.* **52**, 12255–12264 (2018).
17. Nguyen, T. B. et al. Organic aerosol formation from the reactive uptake of isoprene epoxydiols (IEPOX) onto non-acidified inorganic seeds. *Atmos. Chem. Phys.* **14**, 3497–3510 (2014).
18. Surratt, J. D. et al. Reactive intermediates revealed in secondary organic aerosol formation from isoprene. *Proc. Natl Acad. Sci. USA* **107**, 6640–6645 (2010).
19. Lin, Y.-H. et al. Isoprene epoxydiols as precursors to secondary organic aerosol formation: acid-catalyzed reactive uptake studies with authentic compounds. *Environ. Sci. Technol.* **46**, 250–258 (2011).
20. Hu, W. W. et al. Characterization of a real-time tracer for isoprene epoxydiols-derived secondary organic aerosol (IEPOX-SOA) from aerosol mass spectrometer measurements. *Atmos. Chem. Phys.* **15**, 11807–11833 (2015).
21. Surratt, J. D. et al. Chemical composition of secondary organic aerosol formed from the photooxidation of isoprene. *J. Phys. Chem. A.* **110**, 9665–9690 (2006).
22. Kroll, J. H., Ng, N. L., Murphy, S. M., Flagan, R. C. & Seinfeld, J. H. Secondary organic aerosol formation from isoprene photooxidation. *Environ. Sci. Technol.* **40**, 1869–1877 (2006).
23. Nguyen, T. B. et al. Mechanism of the hydroxyl radical oxidation of methacryloyl peroxynitrate (MPAN) and its pathway toward secondary organic aerosol formation in the atmosphere. *Phys. Chem. Chem. Phys.* **17**, 17914–17926 (2015).
24. Xu, L., Kollman, M. S., Song, C., Shilling, J. E. & Ng, N. L. Effects of NOx on the volatility of secondary organic aerosol from isoprene photooxidation. *Environ. Sci. Technol.* **48**, 2253–2262 (2014).
25. Ambro, E. L. et al. Molecular composition and volatility of isoprene photochemical oxidation secondary organic aerosol under low- and high-NOx conditions. *Atmos. Chem. Phys.* **17**, 159–174 (2017).
26. Thornton, J. A. et al. A near-explicit mechanistic evaluation of isoprene photochemical secondary organic aerosol formation and evolution: simulations of multiple chamber experiments with and without added NOx. *ACS Earth Space Chem.* **4**, 1161–1181 (2020).
27. Shilling, J. E. et al. Enhanced SOA formation from mixed anthropogenic and biogenic emissions during the CARES campaign. *Atmos. Chem. Phys.* **13**, 2091–2113 (2013).
28. Setyan, A. et al. Characterization of submicron particles influenced by mixed biogenic and anthropogenic emissions using high-resolution aerosol mass spectrometry: results from CARES. *Atmos. Chem. Phys.* **12**, 8131–8156 (2012).
29. Shrivastava, M. et al. Urban pollution greatly enhances formation of natural aerosols over the Amazon rainforest. *Nat. Commun.* **10**, 1046 (2019).
30. Ding, X. et al. Spatial and seasonal trends in biogenic secondary organic aerosol tracers and water-soluble organic carbon in the southeastern United States. *Environ. Sci. Technol.* **42**, 5171–5176 (2008).

31. Chan, M. N. et al. Characterization and quantification of isoprene-derived epoxydiols in ambient aerosol in the southeastern United States. *Environ. Sci. Technol.* **44**, 4590–4596 (2010).
32. Budisulistiorini, S. H. et al. Examining the effects of anthropogenic emissions on isoprene-derived secondary organic aerosol formation during the 2013 Southern Oxidant and Aerosol Study (SOAS) at the Look Rock, Tennessee ground site. *Atmos. Chem. Phys.* **15**, 8871–8888 (2015).
33. Claeys, M. et al. Formation of secondary organic aerosols from isoprene and its gas-phase oxidation products through reaction with hydrogen peroxide. *Atmos. Environ.* **38**, 4093–4098 (2004).
34. El Haddad, I. et al. Insights into the secondary fraction of the organic aerosol in a Mediterranean urban area: Marseille. *Atmos. Chem. Phys.* **11**, 2059–2079 (2011).
35. He, Q. F. et al. Secondary organic aerosol formation from isoprene epoxides in the Pearl River Delta, South China: IEPOX- and HMML-derived tracers. *J. Geophys. Res. Atmos.* **123**, 6999–7012 (2018).
36. Ding, X., He, Q., Shen, R., Yu, Q. & Wang, X. Spatial distributions of secondary organic aerosols from isoprene, monoterpenes,β-caryophyllene, and aromatics over China during summer. *J. Geophys. Res. Atmos.* **119**, 11,877–811,891 (2014).
37. Chen, X., Hulbert, D. & Shepson, P. B. Measurement of the organic nitrate yield from OH reaction with isoprene. *J. Geophys. Res. Atmos.* **103**, 25563–25568 (1998).
38. Chuong, B. Measurements of the kinetics of the OH-initiated oxidation of isoprene. *J. Geophys. Res*. **107**, ACH 2-1-ACH 2-12 (2002).
39. Sprengnether, M. Product analysis of the OH oxidation of isoprene and 1,3-butadiene in the presence of NO. *J. Geophys. Res*. **107**, ACH 8-1-ACH 8-13 (2002).
40. Lee, B. H. et al. Highly functionalized organic nitrates in the southeast United States: Contribution to secondary organic aerosol and reactive nitrogen budgets. *Proc. Natl Acad. Sci. USA* **113**, 1516–1521 (2016).
41. Xu, Z. N. et al. Multifunctional products of isoprene oxidation in polluted atmosphere and their contribution to SOA. *Geophys. Res. Lett.* **48**, e2020GL089276 (2021).
42. Schwantes, R. H. et al. Low-volatility compounds contribute significantly to isoprene secondary organic aerosol (SOA) under high-NOx conditions. *Atmos. Chem. Phys.* **19**, 7255–7278 (2019).
43. Vasquez, K. T. et al. Rapid hydrolysis of tertiary isoprene nitrate efficiently removes NOx from the atmosphere. *Proc. Natl Acad. Sci. USA* **117**, 33011–33016 (2020).
44. Jacobs, M. I., Burke, W. J. & Elrod, M. J. Kinetics of the reactions of isoprene-derived hydroxynitrates: gas phase epoxide formation and solution phase hydrolysis. *Atmos. Chem. Phys.* **14**, 8933–8946 (2014).
45. Kurtén, T. et al. Alkoxy radical bond scissions explain the anomalously low secondary organic aerosol and organonitrate yields from alpha-pinene + NO3. *J. Phys. Chem. Lett.* **8**, 2826–2834 (2017).
46. Jacobs, M. I., Darer, A. I. & Elrod, M. J. Rate constants and products of the OH reaction with isoprene-derived epoxides. *Environ. Sci. Technol.* **47**, 12868–12876 (2013).
47. Bates, K. H. et al. Gas phase production and loss of isoprene epoxydiols. *J. Phys. Chem. A.* **118**, 1237–1246 (2014).
48. Lee, L., Teng, A. P., Wennberg, P. O., Crounse, J. D. & Cohen, R. C. On rates and mechanisms of OH and O3 reactions with isoprene-derived hydroxy nitrates. *J. Phys. Chem. A.* **118**, 1622–1637 (2014).
49. de Sá, S. S. et al. Influence of urban pollution on the production of organic particulate matter from isoprene epoxydiols in central Amazonia. *Atmos. Chem. Phys.* **17**, 6611–6629 (2017).
50. Newland, M. J. et al. Low-NO atmospheric oxidation pathways in a polluted megacity. *Atmos. Chem. Phys.* **21**, 1613–1625 (2021).
51. Shi, Z. et al. Introduction to the special issue “In-depth study of air pollution sources and processes within Beijing and its surrounding region (APHH-Beijing)”. *Atmos. Chem. Phys.* **19**, 7519–7546 (2019).
52. Whalley, L. K. et al. Evaluating the sensitivity of radical chemistry and ozone formation to ambient VOCs and NOx in Beijing. *Atmos. Chem. Phys.* **21**, 2125–2147 (2021).
53. Vereecken, L. et al. Theoretical and experimental study of peroxy and alkoxy radicals in the NO3-initiated oxidation of isoprene. *Phys. Chem. Chem. Phys.* **23**, 5496–5515 (2021).
54. Novelli, A. et al. Experimental and theoretical study on the impact of a nitrate group on the chemistry of alkoxy radicals. *Phys. Chem. Chem. Phys.* **23**, 5474–5495 (2021).
55. Carlsson, P. T. M. et al. Comparison of isoprene chemical mechanisms under atmospheric night-time conditions in chamber experiments: evidence of hydroperoxy aldehydes and epoxy products from NO3 oxidation. *Atmos. Chem. Phys.* **23**, 3147–3180 (2023).
56. *Gaussian 09, revision A.01* (Gaussian, Inc., 2009).
57. Adler, T. B., Knizia, G. & Werner, H. J. A simple and efficient CCSD(T)-F12 approximation. *J. Chem. Phys.* **127**, 221106 (2007).
58. *MOLPRO, version 2015.1* (MOLPRO, 2015).
59. Holbrook, K. A. P., Robertson, S. H., Robinson, P. J. *Unimolecular reactions*, 2nd ed. (Wiley, 1996).
60. Glowacki, D. R., Liang, C. H., Morley, C., Pilling, M. J. & Robertson, S. H. MESMER: an open-source master equation solver for multi-energy well reactions. *J. Phys. Chem. A.* **116**, 9545–9560 (2012).
61. Gilbert, R. G. & Smith, S. C. *Theory of unimolecular and recombination reactions* (Blackwell Scientific Publications, 1990).
62. Miller, W. H. Tunneling corrections to unimolecular rate constants, with application to formaldehyde. *J. Am. Chem. Soc.* **101**, 6810–6814 (1979).
63. Orlando, J. J. & Tyndall, G. S. Laboratory studies of organic peroxy radical chemistry: an overview with emphasis on recent issues of atmospheric significance. *Chem. Soc. Rev.* **41**, 6294–6317 (2012).
64. Sommariva, R. et al. AtChem (version 1), an open-source box model for the Master Chemical Mechanism. *Geosci. Model. Dev.* **13**, 169–183 (2020).
65. Reeves, C. E. et al. Observations of speciated isoprene nitrates in Beijing: implications for isoprene chemistry. *Atmos. Chem. Phys.* **21**, 6315–6330 (2021).
66. Gaston, C. J. et al. Reactive uptake of an isoprene-derived epoxydiol to submicron aerosol particles. *Environ. Sci. Technol.* **48**, 11178–11186 (2014).
67. Hu, W. et al. Volatility and lifetime against OH heterogeneous reaction of ambient isoprene-epoxydiols-derived secondary organic aerosol (IEPOX-SOA). *Atmos. Chem. Phys.* **16**, 11563–11580 (2016).

Acknowledgements

We thank Lisa Whalley, Dwayne Heard and Eloise Slater from the University of Leeds for providing the HOx data and James Lee from the University of York for the NOx data from the Beijing field campaign. This work was supported by the National Key Research and Development Program of China (2023YFC3709302) and the National Science Foundation of China (41905116/42321003), Guangzhou Municipal Science and Technology Bureau (202206010057), State Key Laboratory of Organic Geochemistry, GIGCAS (SKLOG202124), Department of Chongqing Science and Technology (cstc2021jcyj-msxm0142), and Chengdu Plain Urban Meteorology and Environment Observation and Research Station of Sichuan Province. The Beijing field observations were carried out as part of the Atmospheric Pollution and Human Health (APHH-Beijing) 2017 summer campaign, funded by the UK Natural Environment Research Council, Medical Research Council and Natural Science Foundation of China under the framework of the Newton Innovation Fund (NE/S006648/1 and NE/N007115/1). Additional staff time at York was funded by NERC as part of a APHH phase 2 project (NE/N006917/1).

Author contributions

S.W. carried out the theoretical calculations, and M.J.N. and A.R.R. performed the modeling work. T.J.B., A.M. and C.J.P. provided the measurement data. The first draft of the manuscript was prepared by S.W. and M.J.N. A.R.R., J.F.H., L.W. and X.W. revised the paper. All authors commented on the manuscript.

Competing interests

The authors declare no competing interests.

Additional information

Supplementary information The online version contains supplementary material available at https://doi.org/10.1038/s41612-025-01151-4.

Correspondence and requests for materials should be addressed to Xinming Wang.